DISCRETE PARTICLE SIMULATION OF THE SPREADING PROCESS IN ADDITIVE MANUFACTURING

M.Y. Shaheen[1,2], A.R. Thornton[1], S. Luding[1], T. Weinhart[1]

[1] Multi-Scale Mechanics, Faculty of Engineering Technology, University of Twente
[2] Design, Production and Management, Faculty of Engineering Technology, University of Twente
m.y.shaheen@utwente.nl

Keywords Additive manufacturing, discrete particle simulation, powder layer quality, selective laser melting, spreading process.

Abstract Selective Laser Sintering/Melting (SLS/SLM) are additive manufacturing (AM) technologies. Objects are produced by spreading successive layers of powder material and solidifying selected parts by sintering/melting them with a laser. The focus of this study is the powder spreading process for which the powder characteristics plays a major role for the powder layer quality, that in turn, influences the final product properties.
The spreading process of a characteristic, frequently used, Ti-6Al-4V powder is simulated in MercuryDPM, using a discrete particle model. A parameter study varying cohesion, sliding and rolling friction allows us to quantify the influence of these powder properties on the layer characteristics, such as density and uniformity. The layer characteristics were obtained by coarse-graining, which generates grid-free continuum fields, e.g., density from discrete data. The density and homogeneity of the powder layer decreased with the increase of interparticle friction, leading to non-uniform layer, higher porosity, and dragged particles causing defects in the powder bed. However, the larger interparticle friction led to a rather good bed. In addition, the sliding friction had a little effect on the layer uniformity, but a large effect on particle segregation, whereas the rolling friction had a larger effect on layer uniformity. Further investigations will focus on additional parametric studies, experimental validation, the effect of humidity and spreading tool design evaluation.

1 INTRODUCTION

Additive manufacturing (AM), commonly known as 3D printing, is a manufacturing technology; in contrast to subtractive or formative methods, objects are produced from a three dimensional digital models in a layer-by-layer fashion. AM offers design flexibility and easy customisation that contributed to its rapid growth and wide utilisation in different industrial sectors [1]. Powder bed fusion is a key AM process and includes both

selective laser sintering (SLS) and selective laser melting (SLM).
SLM is mostly applied to metal powder materials and consists of different stages, for each different parameters exist. In SLM objects are produced by spreading successive layers of powder material and solidifying selected parts by sintering/melting them with a laser, Fig. 1 shows a schematic of the process. Optimising the process parameters to achieve the desired final product quality is done by performing costly experimental trials. Developing a computational tool with predictive power would help reducing the amount of trials and thus lower the manufacturing costs and result in better products.

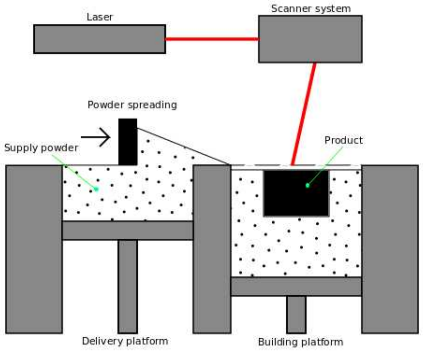

Figure 1: Schematic of the selective laser melting process

The powder spreading process is mainly governed by the geometry, speed, and material properties of the spreading tool. In addition, powder feedstock and powder characteristics play a major role in the powder layer quality, which in turn influences the final product properties and quality. Several previous studies have used the discrete particle method (DPM) to simulate the spreading process to predict the bulk behaviour and investigate particle dynamics. Chen et al. [2] performed a DPM study on the flowing behaviour of powder spreading using a blade as a spreading tool, and found that decreasing either the sliding or rolling friction would decrease the dynamic repose angle and improve flowability. Nan et al. [3] investigated the period and frequency of transient jamming in powder spreading with a small gap height, i.e., the distance between the powder bed and the spreading blade; they defined their relationship with particle properties, blade speed and gap height. Later they studied the powder flow [4], and showed that the mass flow rate through the gap, initially, increases linearly with the gap height until it reaches a limit beyond which the mass flow rate cannot be further increased. Meier et al. introduced a DEM model for cohesion [5] and was able to predict the effective surface energy of Ti-6Al-4V. Then they performed a parametric study, highlighting the effect of cohesion on the spreading process. They introduced quantitative metrics and identified the effect of layer thickness and blade speed on the spread powder layer [6]. Han et al. [7] adapted the approach of [5] to calibrate the surface energy of Hastealloy X (HX) alloy. They focused on the optimization of the layer thickness and validated their results with experiments.

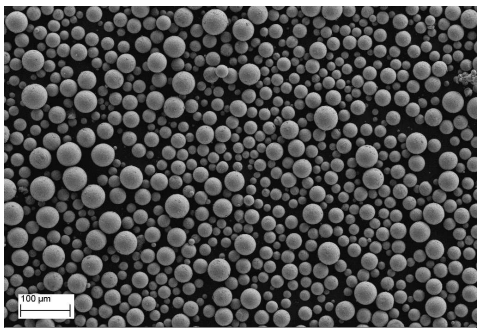

Figure 2: SEM image of Ti-6Al-4V. D10 = 25 μm, D50 = 38 μm, D90 = 57 μm

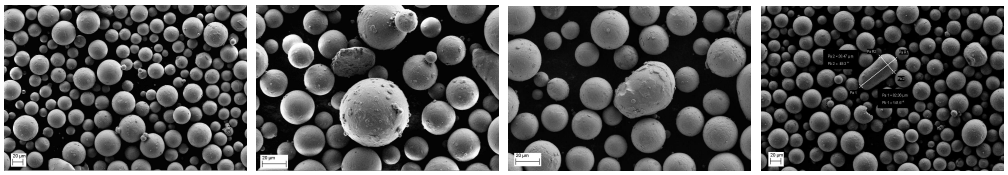

(a) Satellites (b) Rough surface (c) non-sphericity (d) non-sphericity

Figure 3: SEM image of Ti-6Al-4V powder particles irregularities.

The typical size range of metal powder for SLM is D10 = 20-25 and D90 = 50-55 μm (D10 means 10% of particles have a diameter less than D10 value, analogous definition for D90). Spherical shape is favourable in terms of flowability and powder bed packing density, Fig. 2 shows an SEM image of Ti-6Al-4V powder with spherical particles. However, non-sphericity is usually present due to satellites, fracture, adhered particles, etc, as shown in Fig. 3. In addition, metal powders used in SLM tend to behave differently under different conditions, and SLM users have reported different spread-ability of identical powders [8]. This could be due to environmental effects, e.g., powder contamination, oxidation and recycling, in addition to the presence of irregularly shaped particles.
In this work we perform a parametric study on the spreading process of a Ti-6Al-4V powder using DPM simulations. The focus is on the interparticle sliding friction and rolling resistance as a model of irregular particles, mimicking small asperities. In addition, cohesion is included in terms of inter-facial surface energy. This type of quantitative study could provide a guidance for calibration of DPM parameters. A calibration of the model parameters according to the powder material is not performed here. However, the parametric study could be defined as a pre-calibration step, providing an overview about the important parameters relevant to the simulated process. Fig. 4 shows a flow chart of DPM simulation and validation framework. In addition, the process parameters are important input, as they influence the bulk behaviour, hence those need to be set and optimised ensuring good production rate and high products quality. DPM predictions would help in the outlined task, providing an insight into the spread powder characteristics.

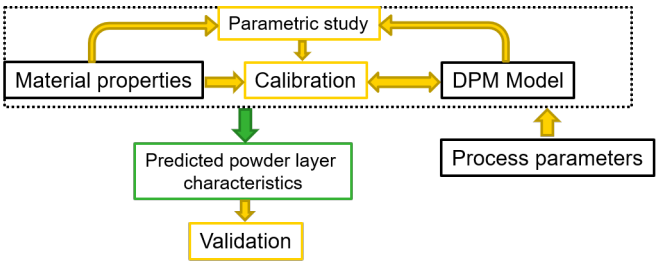

Figure 4: DPM simulation and validation framework

2 METHODS

2.1 Discrete particle method

The discrete particle method is used to simulate the spreading process. The interaction of N poly-disperse particles is modeled using the standard linear spring-dashpot model [9]. Each pair of particles i and j are in contact, if their overlap $\delta_{ij}^n = \max(0, R_i + R_j - |\mathbf{r}_{ij}|)$ is positive, where R_i and R_j are radii of i and j, respectively. $\mathbf{r_{ij}} = \mathbf{r}_i - \mathbf{r}_j$ is the relative distance vector, where $\mathbf{r_i}$ and $\mathbf{r_j}$ are the positions of the particles i and j, respectively. In addition, the particles can interact with the powder bed and spreading tool, which is constructed from polygonal shapes. The normal force (parallel to $\vec{r}_{ij}$) is composed of a linear elastic, linear dissipative and a linear adhesive force:

$$f_{ij}^n = k_n \delta_{ij}^n + \eta_n \nu_{ij}^n + f_{ij}^{adh}, \tag{1}$$

with a normal spring stiffness k_n, damping coefficient η_n, normal relative velocity ν_{ij}^n and a linear adhesion force f_{ij}^{adh} introduced below.
Similarly, the tangential forces (sliding and rolling) are modelled using linear elastic and dissipative forces, where the rolling force is a virtual force, used to calculate the rolling torque. Both the tangential sliding force f^s and rolling torque M^r are assumed to have a yield criteria on, truncating the magnitude of δ^s and δ^r (the sliding and rolling displacements, respectively) as necessary to satisfy: $|f^s| \leq \mu_s |f_{ij}^n - f_{ij}^{adh}|$ and $\mathbf{M}^r = R_{ij}\mathbf{n} \times f^r$ with $|f^r| \leq \mu_r |f_{ij}^n - f_{ij}^{adh}|$, where μ_s and μ_r are the sliding and rolling friction coefficients, respectively. They are usually assumed to be constant (Coulomb type). More details about the contact model can be found in [10, 11, 12, 13].
Many models exist in DPM to describe dry cohesion of small particles, the attractive force due to van der Waals interaction between particles close to each other or in contact. For simplicity, a linear elastic adhesive force law (acting opposite to the normal elastic repulsive force) is used [14].

$$f_{ij}^{adh} = \begin{cases} -f_{max}^{adh} & \delta_{ij}^n \geq 0; \\ -(f_{max}^{adh} + k_{adh}\delta_{ij}^n) & -\frac{f_{max}^{adh}}{k_{adh}} \leq \delta_{ij}^n < 0; \\ 0 & \text{else}, \end{cases} \tag{2}$$

where k_{adh} is the adhesion stiffness during unloading. The maximum adhesion force f_{max}^{adh} is defined identical to the pull-off force of the JKR representation of van der Waals interaction [15]: $f_{max}^{adh} = \frac{3}{2}\pi\gamma R_{eff}$, where γ is the surface energy and $R_{eff} = \frac{R_i R_j}{R_i + R_j}$ is the effective radius of two particles i and j in contact or close proximity.

2.2 Micro-macro transition

To characterise the spread powder layer, continuum fields, e.g., density can be extracted from discrete data using coarse-graining (CG) [17]. This method has the advantage that the fields produced satisfy mass and momentum balance exactly even near the boundaries. In coarse-graining we define macroscopic mass density using a spatial coarse graining function ϕ: $\rho(\mathbf{r}, t) = \sum_{i=1}^{N} m_i \phi(\mathbf{r} - \mathbf{r}_i(t))$. Common coarse graining functions include cutoff Gaussian, Heaviside and Lucy polynomial. Here, we use a Gaussian coarse-graining function of width (standard deviation) w. The evaluated fields depend weakly on the choice of the function [16], and the key parameter is the coarse graining width w.
We now can define the macroscopic volume fraction per unit volume, dividing the mass density by the material density ρ_p: $\Phi = \frac{\rho(\mathbf{r})}{\rho_p}$. More details on the coarse graining method can be found in [16, 17, 18].

3 SPREADING SIMULATION

3.1 Simulation setup

We simulate small part of the powder bed (width 1.5 mm), using periodic boundary condition in the y-direction. The spreading tool is a blade as shown in Fig. 5, moving from left to right at a constant speed v_T. Particles are inserted in the region $(x,y,z) \in [0,0.25] \times [0,2.25] \times [0,h]$ mm^3 until the total particles volume exceeds $0.25 \times 2.25 \times 0.1$ mm^3. h gradually increases (starting at $h = 0$ mm), until all particles are inserted without overlap. After the particles settle down and the system is relaxed, the simulation of the spreading process starts by moving the tool with speed v_T. The simulation thus is spreading the particles in a layer where the tool gap is set to $H = 100$ μm which corresponds to about 2.6×D50 in z-direction. Fig. 5 shows the initial simulation configuration, after inserted particle have settled down.
For the powder layer fields, averaging in z-direction yields spatial coarse graining of the volume fraction per unit volume in xy-directions as $\Phi(x, y)$. The fields were evaluated at the end of the simulation when the system is in a static state. The result is a 2D-map of the depth-averaged volume fraction Φ, as illustrated in the CG figures in Sect. 4.

3.2 Model parameters

The simulations of the spreading process are done using the open-source code MercuryDPM [19, 20, 21]. The same parameter values were set for particle-particle and

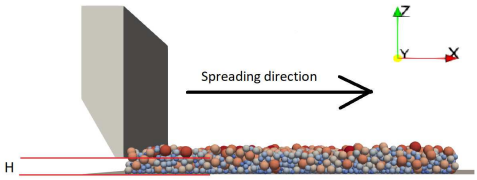

Figure 5: Initial simulation setup

particle-wall interactions. The normal spring k_n and damping η_n constants are set based on the collision time t_c, the smallest particle's mass m_i^{min} and the restitution coefficient ϵ, where the collision time $t_c = t_g/200$ is much smaller than the macroscopic time scale $t_g = \sqrt{D50/g}$, and a small restitution coefficient $\epsilon = 0.1$ is assumed to quickly dampen the velocity fluctuations.

$$\eta_n = -\frac{m_i^{min}}{t_c \log(\epsilon)}, \quad k_n = \frac{1}{2} m_i^{min} \left(\frac{\pi}{t_c}\right)^2 + \left(\frac{\eta_n}{m_i^{min}}\right)^2, \tag{3}$$

The tangential (sliding) spring and damping constants are $k_t^s = (2/7)k^n$ and $\eta_t^s = \eta_n$, such that the frequency of normal and tangential contact oscillation and the normal and tangential dissipation are equal. In addition, the rolling resistance constants are $k_r^t = (2/5)k^n$ and $\eta_r^t = \eta_n$. The microscopic friction coefficients μ_s (sliding friction as a measure of surface roughness) and μ_r (rolling friction as a measure of irregularity in particle shape) are set parametrically as: $\mu_s = 1.0, 0.5, 0.333, 0.25, 0.2, 0$ and $\mu_r = 0.2, 0.1, 0.0667, 0.05, 0.04, 0$. The adhesive force parameters are the surface energy γ and adhesion stiffness, where $\gamma = 0$, 0.1 mJ/m^2 and $k_{adh} = 0, 0.5k_n$. For the cohesivve case, this corresponds to a particle bond number [2]: $K_i = Bo_g = \frac{f_{max}^{adh}}{m_i g} = \frac{9\gamma}{16\rho_p R_i^2 g} \approx 36, 4.5, 0.8$, for $R_i = 6, 17, 40$ μm, respectively; This is consistent with the observation that the effect of cohesion is only moderate in the data presented in Sec. 4.2. The particle size distribution (PSD) of Ti-6Al-4V powder can be fitted to a log-normal type, the PSD was implemented in the simulations as shown in Fig. 6. Computational efficiency could be increased by limiting the PSD in simulations to values between D10 and D90 ignoring the values below D10 and above D90, as done by Meier et al. [6]. However, It is important to implement the full range of particle sizes including the larger and smaller ones, since large ones would tend to cause layer defects and non-uniformity under certain conditions, whereas smaller ones might affect the spreadability or stick to larger ones.

4 RESULTS

4.1 Effect of interparticle friction

First, without cohesion, the rolling friction μ_r was set to zero and only the sliding friction was varied. Then, the sliding friction μ_s was set to zero and only the rolling friction was varied. For all cases, the behaviour was unrealistic. After the particles settle

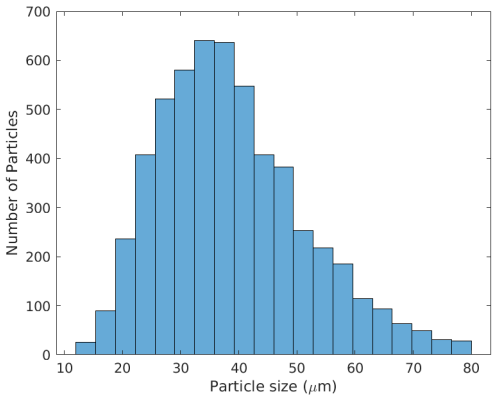

Figure 6: Particle size distribution (diameter) of Ti-6Al-4V as implemented in simulations. D10 = 20 μm, D50 = 38 μm, D90 = 55 μm

Variable	Symbol	Unit	Value	Values range
Particle density	ρ_p	kg/m^3	4430	-
Normal stiffness	k_n	kg/s^2	Eq.(3)	-
Normal dissipation	η_n	kg/s	Eq.(3)	-
Friction stiffness	k_s^t	kg/s^2	$(2/7)k_n$	-
Tangential dissipation	η_s^t	kg/s	$\eta_t^s = \eta_n$	-
Rolling stiffness	k_r^t	kg/s^2	$(2/5)k_n$	-
Rolling dissipation	η_r^t	kg/s	$\eta_t^r = \eta_n$	-
Restitution coefficient	ϵ	-	0.1	-
Sliding friction coefficient	μ_s	-	-	0-1.0
Rolling friction coefficient	μ_r	-	-	0-0.2
Particle diameter	D	μm	12-80	-
Surface energy	γ	mJ/m^2	0.1	0,0.1
Adhesion stiffness	k_{adh}	kg/s^2	$0.5k_n$	$0,0.5k_n$
Width of spreading domain	W	mm	1.5	-
Gap height	H	μm	100	-
Number of particles	N	-	5511	-
Spreading tool speed	v_T	mm/s	-	10,50
Coarse graining width	w	μm	40	-

Table 1: Simulation parameters

(a) $\mu_r = 0$, $\mu_s = 1.0$ (b) $\mu_r = 0.2$, $\mu_s = 0$

Figure 7: Top view of the spreading process at $t = 0.08$ s for $v_T = 10$ mm/s, $\gamma = 0$ mJ/m^2

down, they roll/slide freely, respectively spreading out, with almost no resistance, see Fig. 7. Thus, it is important to set and account for both μ_r and μ_s, i.e., that is perfect spheres give unrealistic behaviour.
Next, the sliding friction and rolling resistance were set as described in Sect. 3.2, with no cohesion. Fig. 8 shows the top view of the spread layer for two different μ_r and μ_s values and the corresponding coarse-graining maps of the volume fraction Φ (per unit volume) of the powder layers. From this figure we can see that at higher rolling friction, meaning particles are more irregular and/or with high surface roughness, the layer is less homogeneous, with high porosity and dragged particles, causing strong defects in the powder bed. Surprisingly the larger μ_r and μ_s leads to a rather good bed. In contrast to the bad deposition at intermediate rolling friction values, see Fig. 8(c), (e) and (g), at the highest interparticle friction, the segregation mechanism during spreading changes such that bigger particles accumulate in the low shearing region, at the top of the particles avalanche (not shown), and thus the deposited layer consists initially of small particles, see Fig. 8(a).

4.2 Effect of cohesion

Next, we include cohesion as described in Sect.2.1. The interparticle friction effect on cohesive particles, was similar to non-cohesive ones. At high rolling resistance the layer was nonuniform, higher porosity and with particle drag. In Fig. 9, we see an example of volume fraction Φ map at low and high rolling friction.
Foster et al. [22] reviewed common defects in powder bed fusion processes, one is particle drag during powder spreading, which is confirmed by our simulation results at higher rolling resistance (but not the highest μ_r and μ_s), which is interpreted as a measure of irregularity in particles shape that includes non-sphericity, contamination, satellites, etc; Fig. 10 shows some of the powder bed defects.

5 CONCLUSION & OUTLOOK

The spreading process was simulated in MercuryDPM [19, 20, 21] using the discrete element method. Particle scale simulations of the process provide information on the powder flow behaviour and layer quality, which is essential before the sintering/melting process. The qualitative study showed that high interparticle friction as a measure of particle irregularities (μ_s as surface roughness and μ_r as particle shape) would lead to non-uniform layers, higher porosity, and dragged particles causing defects in the powder

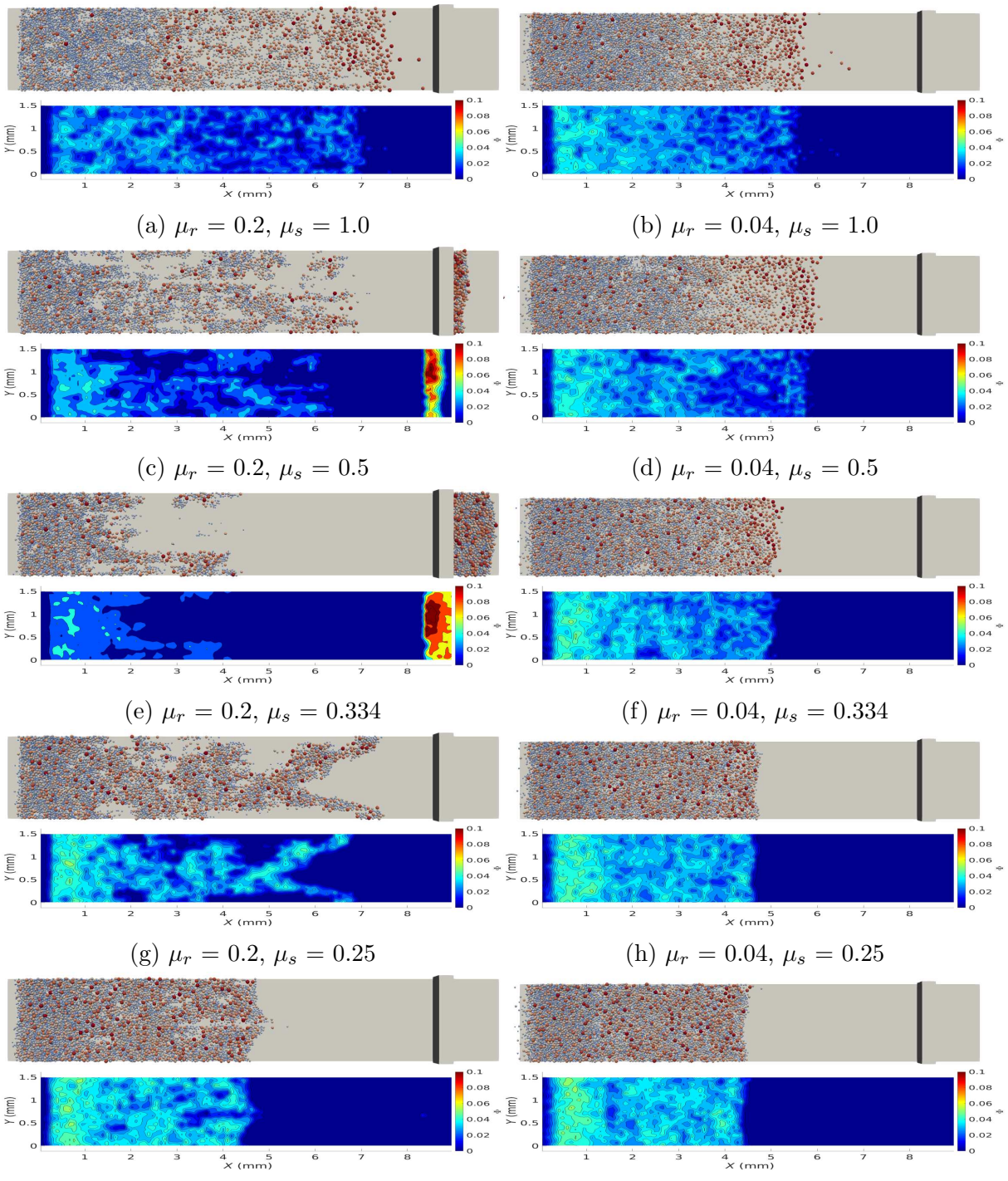

(a) $\mu_r = 0.2$, $\mu_s = 1.0$ (b) $\mu_r = 0.04$, $\mu_s = 1.0$

(c) $\mu_r = 0.2$, $\mu_s = 0.5$ (d) $\mu_r = 0.04$, $\mu_s = 0.5$

(e) $\mu_r = 0.2$, $\mu_s = 0.334$ (f) $\mu_r = 0.04$, $\mu_s = 0.334$

(g) $\mu_r = 0.2$, $\mu_s = 0.25$ (h) $\mu_r = 0.04$, $\mu_s = 0.25$

(i) $\mu_r = 0.2$, $\mu_s = 0.2$ (j) $\mu_r = 0.04$, $\mu_s = 0.2$

Figure 8: Top view of the spread layer and corresponding CG map of layer volume fraction Φ per unit volume (in different scale), for $v_T = 10$ mm/s, $\gamma = 0$ mJ/m^2 and $Bo_g = 0$

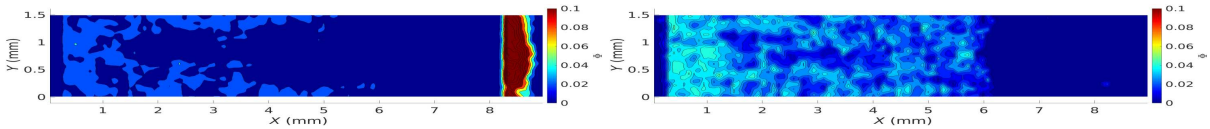

(a) $\mu_r = 0.2$, $\mu_s = 0.5$ (b) $\mu_r = 0.04$, $\mu_s = 0.5$

Figure 9: CG map of layer volume fraction Φ per unit volume, with $v_T = 10$ mm/s, $\gamma = 0.1$ mJ/m^2

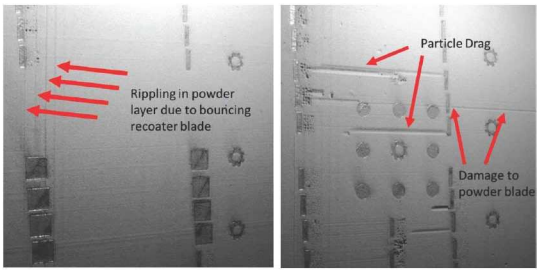

Figure 10: Powder bed defects (courtesy of Foster et al. [22])

bed. On top of that, cohesion is important for qualitative calibration. In addition, μ_s had a little effect on the layer uniformity, but a large effect on particle segregation, whereas μ_r had a larger effect on layer uniformity. The spreading process parameters play a role for the layer quality, too, which in turn influences the final product properties. Increasing the tool speed from $v_T = 10$ mm/s to $v_T = 50$ mm/s has increased the layer porosity for almost all the cases.

The current simulation setup (i.e. number of particles) was suitable for a qualitative understanding. More particles are needed to quantify the effects on uniformity and segregation, where the standard deviation of $\Phi(x, y)$ can be used as a measure of the layer uniformity. In addition, parametric studies in terms of both surface energy and interparticle friction should be carried out, since irregularity and asperities would influence the effective surface energy as well. Beside that, further investigations of the effect of process parameters on the particle dynamics during the spreading process should be done, as optimising those might overcome some of the defects in the powder bed caused by powder properties. In addition, it is important to obtain as much information as possible about the significance of the powder properties to the process. One of the things that could be done to minimise the irregularity in the powder is to sieve it to a specified sieve grid size multiple times, which would reduce the number of irregular particles. Finally, experimental calibration and validation are needed next.

6 ACKNOWLEDGMENT

This work was financially supported by NWO-TTW project 15050 Multiscale modelling of agglomeration: Application to tabletting and selective laser sintering.

REFERENCES

[1] Ngo, T. D., Kashani, A., Imbalzano, G., Nguyen, K. T. Q., & Hui, D. (2018). Additive manufacturing (3D printing): A review of materials, methods, applications and challenges. Composites Part B: Engineering. Elsevier.

[2] Chen, H., Wei, Q., Wen, S., Li, Z., & Shi, Y. (2017). Flow behavior of powder particles in layering process of selective laser melting: Numerical modeling and experimental verification based on discrete element method. International Journal of Machine Tools and Manufacture, 123, 146-159.

[3] Nan, W., Pasha, M., Bonakdar, T., Lopez, A., Zafar, U., Nadimi, S., & Ghadiri, M. (2018). Jamming during particle spreading in additive manufacturing. Powder Technology, 338, 253-262.

[4] Nan, W., & Ghadiri, M. (2019). Numerical simulation of powder flow during spreading in additive manufacturing. Powder Technology, 342, 801-807.

[5] Meier, C., Weissbach, R., Weinberg, J., Wall, W. A., & John Hart, A. (2019). Modeling and characterization of cohesion in fine metal powders with a focus on additive manufacturing process simulations. Powder Technology, 343, 855-866.

[6] Meier, C., Weissbach, R., Weinberg, J., Wall, W. A., & Hart, A. J. (2019). Critical influences of particle size and adhesion on the powder layer uniformity in metal additive manufacturing. Journal of Materials Processing Technology, 266, 484-501.

[7] Han, Q., Gu, H., & Setchi, R. (2019). Discrete element simulation of powder layer thickness in laser additive manufacturing. Powder Technology, 352, 91-102.

[8] King, W., 2017. Modeling of Powder Dynamics in Metal Additive Manufacturing: Final Powder Dynamics Meeting Report. https://hpc4mfg.llnl.gov/events-powderdynamics2017.php.

[9] Cundall, P.A., Strack, O.D.L.: A discrete numerical model for granular assemblies. Geotechnique 29, 47-65 (1979)

[10] Luding, S.: Introduction to discrete element methods: basics of contact force models and how to perform the micro-marco transition to continuum theory. Eur. J. Environ. Civ. Eng. 12(7-8), 785-826 (2008)

[11] Luding, S. (2008). Cohesive, frictional powders: Contact models for tension. Granular Matter, 10(4), 235-246.

[12] Weinhart, T., Thornton, A. R., Luding, S., & Bokhove, O. (2012). Closure relations for shallow granular flows from particle simulations. Granular Matter, 14(4), 531-552.

[13] Fuchs, R., Weinhart, T., Meyer, J., Zhuang, H., Staedler, T., Jiang, X., & Luding, S. (2014). Rolling, sliding and torsion of micron-sized silica particles: Experimental, numerical and theoretical analysis. Granular Matter, 16(3), 281-297.

[14] Roy, S., Singh, A., Luding, S., & Weinhart, T. (2016). Micromacro transition and simplified contact models for wet granular materials. Computational Particle Mechanics, 3(4), 449-462.

[15] Johnson, K. L., Kendall, K., & Roberts, A. D. (1971). Surface Energy and the Contact of Elastic Solids. Proceedings of the Royal Society A: Mathematical, Physical and Engineering Sciences, 324(1558), 301-313.

[16] Goldhirsch, I. (2010). Stress, stress asymmetry and couple stress: from discrete particles to continuous fields. Granular Matter, 12(3), 239-252.

[17] Weinhart, T., Thornton, A. R., Luding, S., & Bokhove, O. (2012). From discrete particles to continuum fields near a boundary. Granular Matter, 14(2), 289-294.

[18] Tunuguntla, D. R., Thornton, A. R., & Weinhart, T. (2016). From discrete elements to continuum fields: Extension to bidisperse systems. Computational Particle Mechanics, 3(3), 349-365.

[19] Weinhart, T., Post, M., Orefice, L., Tsang, J., Rapino, P., Polman, H., Roy, S., Shaheen, M. Y., Naranjo, J., Grannonio, E., Cheng, H., Denissen, I., Shi, H., Barbosa, J., Jing, L., den Otter, W., & Thornton, A. R. (2019). Fast, flexible particle simulations: an introduction to MercuryDPM. Proceedings of the 8th International Conference on Discrete Element Methods.

[20] Thornton, A.R., Krijgsman, D., te Voortwis, A., Ogarko, V., Luding, S., Fransen, R., Gonzalez, S.I., Bokhove, O., Imole, O., & Weinhart, T. (2013). A review of recent work on the Discrete Particle Method at the University of Twente: An introduction to the open- source package MercuryDPM. Proceedings 6th Conference on Discrete Element Methods.

[21] Thornton, A.R., Krijgsman, D., Fransen, R., Gonzalez, S.I., Tunuguntla, D., te Voortwis, A., Luding, S., Bokhove, O., & Weinhart, T. (2013). Mercury-DPM: Fast particle simulations in complex geometries, EnginSoft Year 10, No. 1.

[22] Foster, B. K., Reutzel, E. W., Nassar, A. R., Dickman, C. J., & Hall, B. T. (2015). A brief survey of sensing for metal-based powder bed fusion additive manufacturing. In K. G. Harding & T. Yoshizawa (Eds.), Dimensional Optical Metrology and Inspection for Practical Applications IV (Vol. 9489, p. 94890B).